Hindawi
International Journal of Distributed Sensor Networks
Volume 2024, Article ID 5562848, 19 pages
https://doi.org/10.1155/2024/5562848

Research Article

A Photothermal Modelling Approach for Micro-LED Arrays in Wireless Optogenetics

Yanping Ji,[1] **Chuanzhen Liu**,[1] **Jiawei Li**,[1] **Wensi Wang**,[1] **and Mengyi Zheng**[2]

[1]*Faculty of Information Technology, Beijing University of Technology, Beijing 100124, China*
[2]*School of Sociology, China University of Political Science and Law, Beijing 100091, China*

Correspondence should be addressed to Wensi Wang; wensiwang1@163.com and Mengyi Zheng; zhh_jyp361@163.com

Received 24 November 2023; Revised 29 February 2024; Accepted 8 March 2024; Published 16 April 2024

Academic Editor: Saeed Olyaee

Implantable LED light sources have received a lot of attention in the field of optogenetic neuromodulation. This type of light modulation enables effective stimulation of neurons. However, as optogenetics moves towards clinical trials, combinatorial photostimulation based on arrays of LED light sources has emerged. This approach inevitably brings about a large increase in transient temperature, resulting in the inability to achieve precise stimulation of cells. We designed a wireless optogenetic hardware system to realize the control of the stimulation mode and temperature of the light source array. At the same time, a set of combined photothermal physical model was established to simulate the photothermal response of the whole experiment. The physical model can effectively guide the wireless optogenetic hardware circuits to perform effective stimulation within a controlled temperature range. Our model provides a new technical approach for photothermal studies in optogenetic clinical trials.

1. Introduction

Optogenetics (OG) is an approach to neuromodulation and brain science that combines optics and genetics. The idea is to first "insert" a light-sensitive ion channel protein into a nonvirulent adeno-associated virus (AAV) using recombinant DNA technology. The adenovirus is then injected into the study cells, where the specific neuronal cells are infected and form light-sensitive ion channels in their cell membranes. The light-controlled "on/off" of the neuronal light-sensitive ion channels is then achieved by irradiation with a characteristic spectral light source, enabling light-controlled neuromodulation. Perhaps, more importantly for neuromodulation and biomedical engineering is the application of this technology to clinical practice. Indeed, with the rapid advancements in neuromodulation technology, electrical stimulation has emerged as the primary modality used in medical applications. Techniques such as deep brain stimulation (DBS), vagus nerve stimulation (VNS), sacral nerve stimulation (SNS), and spinal cord peripheral stimulation (SCS) have been extensively utilized to treat various neurological disorders. These disorders include Parkinson's disease, epilepsy, neurogenic incontinence, and intractable or cancer-related pain, among others. These stimulation techniques have significantly contributed to the relief of patients' suffering and have shown promising results in improving their overall well-being [1]. Optogenetics techniques offer distinct advantages over neuroelectrical stimulation in terms of modulation specificity and spatial precision for neurons and diseases. Optogenetics provides the ability to precisely control and manipulate specific neurons using light-sensitive proteins, allowing for targeted and precise modulation of neural activity. This level of precision can potentially lead to more effective and personalized treatments for neuromodulatory disorders. There are already research teams actively working on optogenetic technology and conducting scientific studies to explore its potential clinical applications. These studies are aimed at investigating the feasibility and efficacy of optogenetics in treating the neuromodulatory disorders mentioned earlier. These ongoing efforts hold great

promise for the future of optogenetics as a potential therapeutic approach [2].

The commonly used optogenetic light source tools are often based on laser and fiber optic technology. For instance, the Changchun Institute of Optomechanics, Chinese Academy of Sciences, has developed a laser and implantable fiber optic pin kit for optogenetic research [3]. This technology is well-established and mature. As long as the stimulation threshold for such light sources is maintained above a moderate level, power consumption and heat dissipation are typically not major concerns. In contrast, the use of LEDs as light sources for clinical medical experiments in optogenetics neuromodulation is still relatively in its early stages of development. When employing LEDs as light sources in optogenetic experiments, there are two main design approaches to consider. The first approach involves utilizing a light waveguide technique. In this approach, the light source is generated away from the tissue and then delivered to the target neuron via a light waveguide delivery system. The second approach involves localised light stimulation, where the LED directly stimulates the targeted neuron without the need for a waveguide or delivery system. Both approaches have their advantages and considerations, and the choice between them depends on the specific requirements of the experiment or application. Continued research and advancements in LED-based optogenetic light sources are expected to further enhance their capabilities and effectiveness in clinical settings.

In terms of the process of light stimulation, for the neurons to be effectively stimulated, they must be given sufficient light intensity. Cultured cells encoded with wild-type ChR2 typically require photon fluxes of 10^{17}–$10^{19}\,s^{-1}\,cm^{-2}$ (0.4-40 mW/mm^2) to achieve a full dynamic range of photocurrent response [4–6]. Typically, reliable neural firing at 20 Hz has required 0.7 mW/mm^2. This optical power parameter enables optimal photostimulation response in optogenetic studies by Prof. Sheng Xing's team. Meanwhile, in a study targeting optogenetics and dopamine detection studied by Sheng Xing et al. Radiance in vivo between 10^{16}-10^{19} photons between $s^{-1}\,cm^{-2}$ (40uW/mm^2-40 mW/mm^2) [7, 8]. The intensity of radiation inside the body is slightly lower compared to outside the body. Depending on the requirements of in vivo and in vitro studies of neuronal cells, there is a need for our light source array probes to be able to adapt to the appropriate light intensities. At the same time, variant structures on ChR2 are constantly being adapted to changes in parameters such as light intensity faster and more efficiently [9]. Considerable efforts have been made by scientific scholars in this area. CatCh protein, a variant of the light-sensitive protein ChR2, which reduces the amount of photons in response to Ca^{2+}-derived light stimulation to 10^{16}-10^{17} photons $s^{-1}\,cm^{-2}$ [10, 11]. Thus, we can see that the binding of different light-sensitive proteins to different neuronal cells requires us to design different thresholds for photostimulation parameters. Opsins are generally responsive to high-energy and low-penetration depth visible wavelengths. Fiber optics that are used to deliver light close to the target cells located in the deeper regions have disadvantages including artifacts and inconveniences in moving animal experiments. Therefore, wireless methods are of interests in neuromodulation both in label-free approaches and optogenetics as a labeled strategy. Wireless approaches include use of plasmonic materials and upconversion materials when using highly penetrated NIR light sources, or use of implanted micro-LEDs [12, 13].

It is possible that localised light stimulation techniques offer more advantages over optical waveguide technology systems with different thresholds. Localised light stimulation allows for the multiplexing of light sources, enabling the adjustment of different light intensities. This flexibility in adjusting light intensities is beneficial for experimental setups, as it provides finer control over the stimulation parameters. Moreover, the effective integration of control circuitry with the light source enables wireless stimulation. This eliminates the need for physical connections and offers greater freedom and convenience in experimental designs. The ability to stimulate wirelessly simplifies the experimental procedures and enhances the feasibility of optogenetic applications in various settings. By utilizing localised light stimulation techniques, researchers can achieve precise control over neural activity and conduct more sophisticated experiments. The wireless capability and multiplexing of light intensities open up new possibilities for studying and treating neurological disorders with improved precision and adaptability [14].

However, for LED light sources and micro-LED light sources, even the best light efficiency can only reach 80%. This may not meet the 2 degree Celsius temperature limit on the surface of the light source if the control parameters of the control circuit are not precise. If the temperature limit of 2 degrees Celsius is to be guaranteed, it is possible that for specific biological tissues, their light intensity will not reach the state of activation of nerve cells. The key issue is therefore to find a balance between light intensity and temperature limit. The current research team focuses on the device characteristics and thermal features of the light source itself; for example, Mcalinden et al. discussed the optical and thermal characterization of their respective monolithic gallium nitride optrode [15]. However, no team has yet designed an optogenetic photothermal model with an optimal combination of light source arrays, light intensity, temperature limits, and hardware association from the perspective of photothermogenesis.

Based on existing research, this system designs and flows a micro-LED array for optogenetics and a wireless optogenetic control circuit. And the physical model was established on light and heat in the experiment to verify the optimal photothermal relationship, and the wireless optogenetic parameter optimisation algorithm is designed to achieve the optimisation of the parameters of the whole system.

2. Methodology

The overall structure of the system is shown in Figure 1, where Figure 1(a) shows the wireless optogenetic micro-LED array stimulation circuit we designed, Figure 1(b) shows the wireless power supply circuit, Figure 1(c) shows the customised Petri dish we designed, Figure 1(d) shows

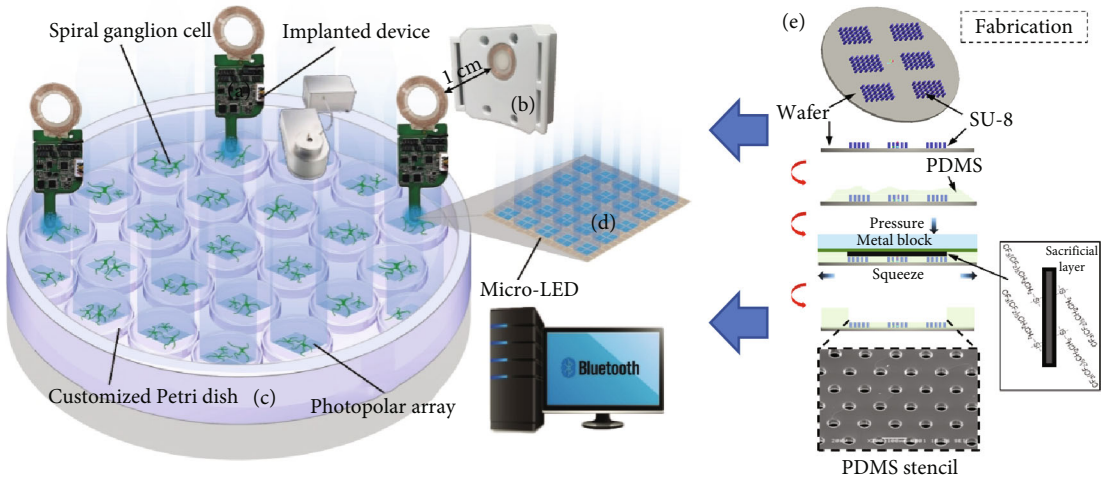

FIGURE 1: System overall structure diagram: (a) wireless optogenetic micro-LED array stimulation circuit; (b) wireless power supply circuit; (c) customised Petri dish; (d) structure of the light source array; (e) structure of the customised Petri dish.

the structure of the light source array we designed, and Figure 1(e) shows the structure of the customised Petri dish we designed. Our physical model is centred around the whole experiment.

2.1. Wireless Optogenetic Circuit LED

2.1.1. Micro-LED Photopolar Array Design. The micro-LED array used in this system was designed using GaN. In order to achieve a more precise irradiation of the neurons, a smaller array of light poles was designed. Smaller LEDs will, therefore, require higher drive current densities to achieve the same emission profile. However, this means that they are more susceptible to droop. Droop is a phenomenon well documented within the LED community whereby the efficiency has an inverse relationship with the current density. It was recently attributed to the Auger recombination by Iveland et al. Figure 2(a) compares the luminous efficacy of mini LEDs and micro-LEDs (Cree Crop DA2432, light-emitting surface: 280 μm × 210 μm) from literature [16] and literature [17]. The comparison shows that the emission efficiency of micro-LEDs, despite being relatively low, is sufficient for the light excitation intensity of neurons, and taking into account the thermal implications, we ultimately chose to design micro-LED arrays. We fitted the input power versus radiation flux parameters for different sizes of micro-LED single light sources, as shown in Figure 2(b). Thus, the radiant flux can be considered as another element of the light source. It should be noted here that the requirement for light intensity in our optogenetic experiments is about 8 mW/mm^2. Considering the luminous efficiency of micro-LEDs, we finally chose micro-LED arrays with a single size of 60 μm size. Later, hardware experiments also verified that choosing 60 μm size can meet the requirements.

As it can also be seen in Figure 2(b), for micro-LEDs, the turn-on voltage is set at around 2.5 V-3.5 V and the current is set at 100 mA or less. With these preset basic elements, the micro-LED array is designed and flow sheeted. The electrical, optical, and thermal properties and circular micro-LEDs with equal light-emitting area in the light source size range of 30-100 μm were tested in the first stage; the influence of the shape of the light-emitting area on the characteristics of the micro-LEDs at different sizes was studied in comparison, and a single micro-LED light source with a square light source size of 60 μm was selected, taking into account its photoelectric and thermal properties. When the micro-LED current is injected into the active area, the radiation compound photons will spill out from all directions; in order to avoid the interference between pixels and improve the external quantum efficiency, electrical and optical isolation is required, and the simplest way is to carry out etched isolation trench design. The easiest way to do this is by etching isolated trenches, which are formed by etching or etching N-GaN onto a sapphire substrate to form mutually independent light-emitting units. The epitaxial wafer used for array preparation is GaN, where the process includes mesa (etching of the light-emitting region), ISO (etching of the isolation trench), ITO (vapour deposition of the ITO current extension layer), Nline (sputtering of the N electrode), PV (preparation of the passivation layer), and Pline (sputtering of the P electrode), and for subsequent soldering of the bare core using the COB package, the N pole of the light source is selected on one side of the preparation. The process of preparing the 8 × 8 optical array is shown in Figure 2(c).

In Figure 2(c), first clean the epitaxial wafer; remove the surface metal oxides and residual impurity particles; start the first step mesa, that is, the luminescent area etching, using bright field mask version and positive photoresist UV lithography, through ICP dry etching process; and complete the luminescent area photolithography version of the graphic transfer; the second step is the isolation tank ISO etching, using dry etching N-GaN to the sapphire substrate, etching depth of 4.5 μm, to prevent intercell conductivity and luminescence through NGaN; the third step is the ITO transparent conductive layer, through the electron beam evaporation of 110 nm ITO, ITO etching solution to remove the excess, to complete the graphic transfer of the ITO photolithography plate; the fourth step is the interconnection N electrode,

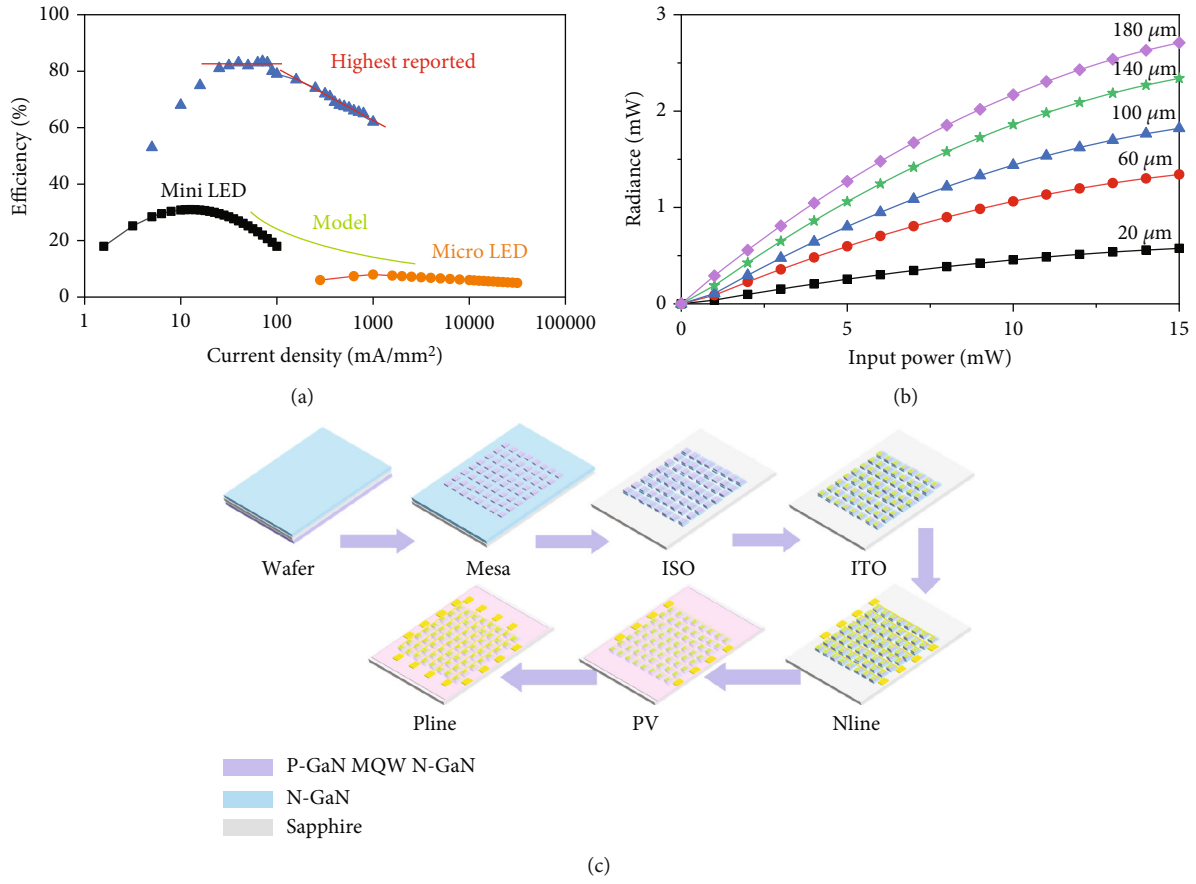

Figure 2: Electro-optical conversion efficiency of LEDs: (a) measured efficiencies from mini LEDs, micro-LEDs, and an empirical model of what is currently available [18]. Also plotted is the highest reported LEDs in the literature [19]. (b) Assuming the model in (a), the radiance vs. input power profile for different LED sizes; (c) process flow for micro-LED passive arrays.

through the electron beam evaporation of 2.4 μm thick Cr/Al/Ti/Pt/Au, a total of 11 layers of metal as the N electrode. The P and N electrodes also need to be insulated between the positive and negative electrodes to avoid short circuit problems, but the oxide has poor adhesion on the metal surface and is prone to cracking or even falling off during preparation. So the surface metal of the multilayer metal is Cr to increase the adhesion of the N electrode to the SiO_2 insulating layer; the fifth step is PV insulating layer or passivation layer, grow a layer of 1000 nm thick SiO_2 by PECVD, and use dark field mask version and positive photoresist lithography etching solution to remove the excess part of SiO_2 to achieve the light-emitting area and N electrode solder joint window; the sixth step is the interconnection P electrode, and use bright field mask version and negative photoresist lithography, with vapour deposition of 2.4 μm thick Cr/Al/Ti/Pt/Au, a total of 9 layers of metal as P electrode by thermal evaporation; the first layer of multilayer metal in contact with SiO_2 is also made of Cr first to increase the adhesion of P electrode on SiO_2 and array interconnection N electrode. The prepared chip is thinned and back-plated with a DBR reflective layer to improve the light extraction efficiency. Figure 3(a) shows a micrograph of a successfully prepared bare core of a passive array of micro-LEDs with a pixel size of 60 μm × 60 μm.

2.1.2. Wireless Optogenetic Micro-LED Array Stimulation Circuit. The internal structure of the implanted circuit is shown in Figure 3(b). In previous research and development, our team has successfully developed a near-field magnetic coupling wireless power transfer (WPT) technology with an operating frequency of 13.56 MHz. This technology enables power transmission within a distance of approximately 10 millimeters, meeting the requirements for subcutaneous implantation. The coil, with a diameter of 28 millimeters, is wound with three strands of pure gold wire and protected by silicone gel. It receives energy from an external power supply circuit through coil coupling. Initially, this energy is converted from AC to DC through an AC-DC power circuit. Then, it is further transformed into low-voltage DC power current (DC-DC) to provide a stable output of 3.3 V power voltage required by various modules. The control chip of the implanted circuit adopts Nordic's nRF52832 series SoC chip, which has a minimum package size of only 2.7 mm × 2.7 mm. It integrates an STM32M4F class processor and 2.4 GHz wireless communication, and the wireless communication chip is compatible with the BLE Bluetooth protocol. This controller has been prevalidated in the medical implantation circuit of our research group, meeting the basic implantation requirements. The controller controls two parts of the chip. The first part is

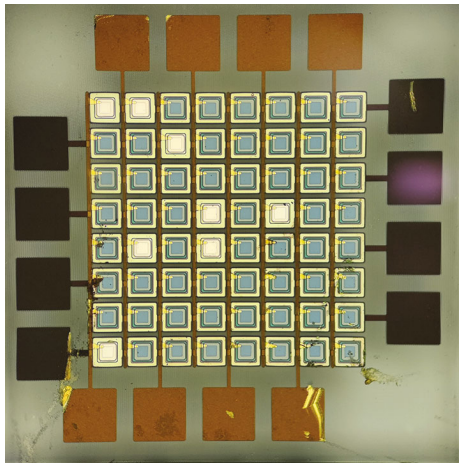

(a)

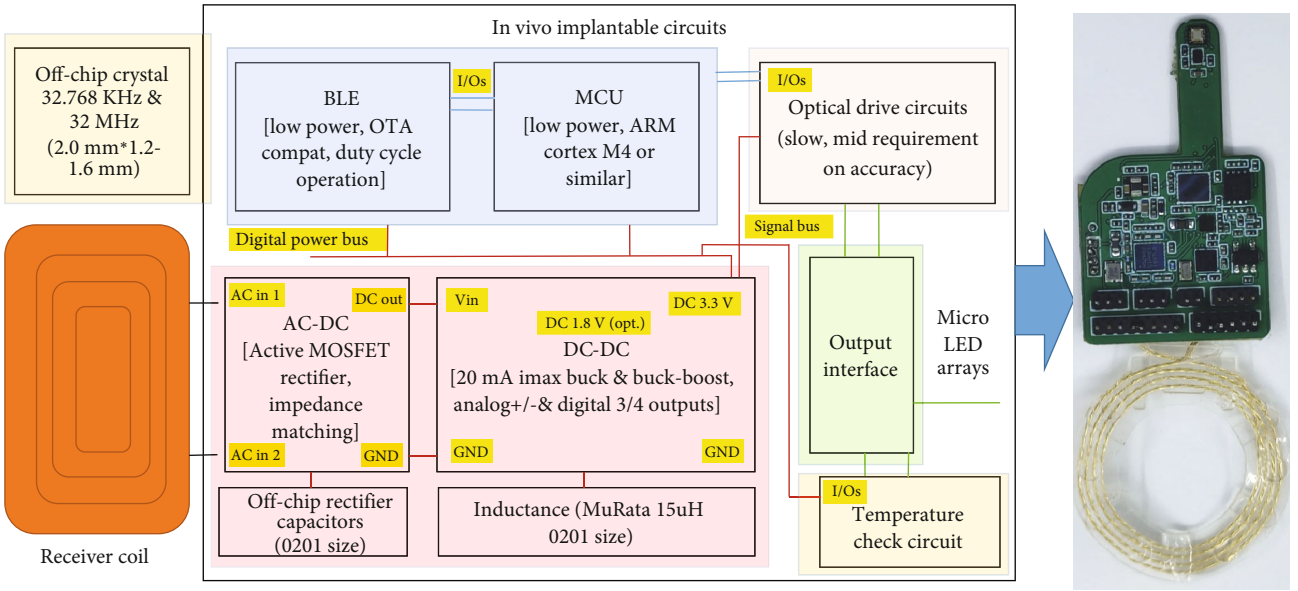

(b)

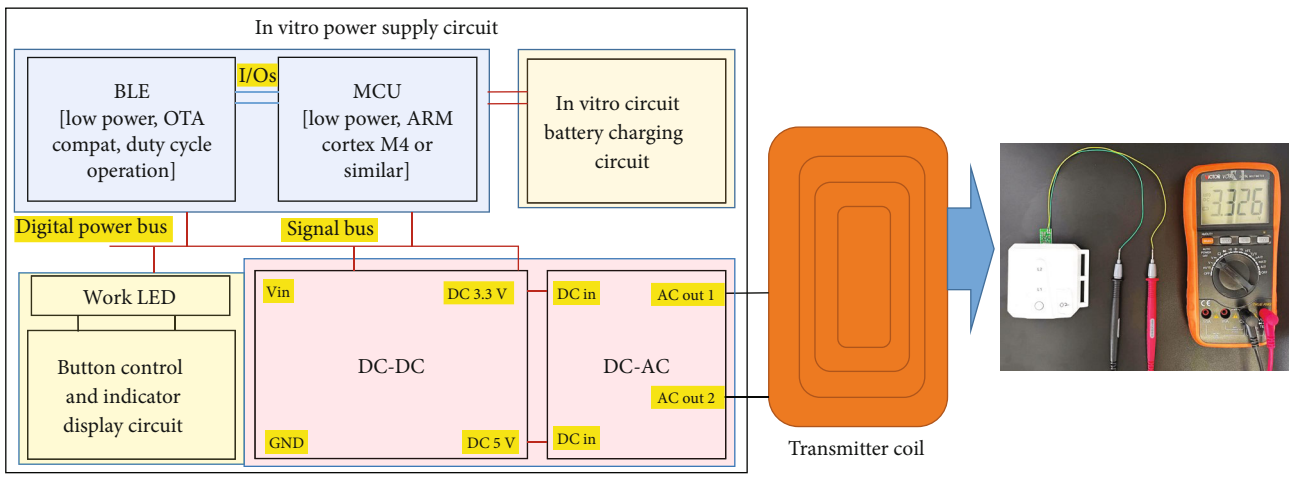

(c)

Figure 3: (a) Micro-LED micrograph. (b) Wireless optogenetic micro-LED array stimulation circuit structure and test object diagram. (c) in vitro wireless power circuit.

Table 1: Measured coil parameters at 13.56 MHz.

Coil parameter	Transmitter coil	Receiver coil	Receiving coil with load 1.5 Ω
Inductors	4.30 μH	1.52 μH	1.68 μH
Equivalent resonant capacitance	129 pF	347 pF	334 pF
Resistor	0.89 Ω	0.36 Ω	1.96 Ω
Quality factor Q	204	182	36

the light driving chip, which uses the STLED524 driver chip and pulse width modulation (PWM) technology to achieve single or multiple point illumination of the light source. The second part is the temperature detection chip. Considering the heat generated by the implant, a temperature detection circuit is added at the location of the light source array. This circuit uses the TMP117 chip and peripheral circuit design to achieve high-precision temperature detection while meeting the long-term implantation requirements. The physical diagram of the designed implanted circuit is shown on the right side of Figure 3(b). The specific circuit has a detailed circuit diagram in Figure S1.

2.1.3. In Vitro Wireless Power Circuit. The overall structure of the in vitro wireless power circuit is illustrated in Figure 3(c). The technical idea of the whole wireless power supply circuit is shown on the left side of Figure 3(c). The right side of Figure 3(c) shows the entire physical object and the test results after removing the wireless power supply circuit alone. It can be seen that the wireless receives 3.3 V, which meets the requirements of our in vivo power supply. An enclosure is designed for the power management circuitry. The lower portion of the enclosure contains the backside wireless energy transmission section, where the coils are embedded on the surface and secured with silicone gel. To achieve stable control of the power supply voltage in the external circuit, the same controller used for the in vivo implantation circuit is employed, eliminating the need for redundancy. Additionally, the circuit includes the design of buttons and an LED display circuit. A battery stabilization charging circuit is designed to charge the internal battery from the external power supply. This circuit filters and removes noise from the input power source and divides the voltage into 3.3 V and 5 V, preparing them for power supply to the internal circuit and wireless power transmission. When the charging is complete, pressing and holding the button for 10 seconds activates the entire external power supply. The green LED indicator light flashes, and the internal circuit converts the DC voltage to 5 V through DC-DC voltage regulation. It is then transmitted to the coil through DC-AC conversion, allowing for power coupling and supply to the internal coil. The specific circuit has a detailed circuit diagram in Figure S2.

Table 1 lists the results of parameter measurements based on the impedance analyser WK6500 transmitter and receiver coils. The optimum theoretical value of the load was previously obtained as 1.3, and the experimental value of the load resistance was 1.5 for better experimental operation and data analysis. Since the ESR measurement of the coils is very sensitive to the surrounding environment and the position of the coil terminals connected to the impedance analyser, the parameter measurements of the experimental coils were carried out with the addition of resonant capacitor tuning, which reduces the experimental measurement errors. Through the whole experimental measurement results, it can be seen that the quality factor conforms to the whole test results.

2.2. Micro-LED Array Simulation Analysis

2.2.1. Analysis of Micro-LED Array Optical Parameters. Modelling of a designed micro-LED array is an efficient way to control the parameters of a wireless optogenetic circuit. We can use the modelling method to analyse the parameters that affect the stimulation of the opsins including the luminescence characteristics of the light source, the spatial distribution, and the spatial light intensity distribution. At the same time, the effect of different light wavelengths on light-sensitive proteins of future optogenetics can be extended [20]. In this paper, we simulate the light illumination of a 470 nm array of blue light. It is important to simulate parameters such as the size of the light source, the spacing between the light sources, and the light intensity distribution, as all these parameters affect the stimulation response of the biological tissue. Therefore, an algorithmic model of optical distribution of light in biological tissues was designed in MATLAB for this system. The model is used to initially determine the parameters of our light source. We designed our light source as a micro-LED, taking full account of the fact that small size enables effective and precise stimulation of neurons. Ideally, the micro-LED can be regarded as a Lambertian [21] body, and the light emitted from the light-emitting surface of the chip conforms to the Lambertian cosine theorem, and the light intensity can be expressed as

$$L(\theta) = L_\theta \cos^n \theta, \tag{1}$$

where θ is the luminous angle, L_θ is the light intensity of the micro-LED on the extended optical axis, and the value of n depends on the micro-LED half-intensity angle $\theta_{1/2}$, which is related as follows:

$$n = \frac{-\mathrm{In}2}{\mathrm{In}(\cos \theta_{1/2})}. \tag{2}$$

As the size of the micro-LED is much smaller than the distance from the light source to the working surface, the micro-LED can be regarded as a point source, with an illumination of

$$I(R,\theta) = \frac{L(\theta)}{R^2} = \frac{L_0 \cos^n\theta}{R^2}, \tag{3}$$

where R is the distance from the micro-LED to the working surface, converted to a right angle coordinate system; the illuminance from the LED source in the xy plane to any point $P(x, y, z)$ in the plane can be expressed as

$$E(x,y,z) = \frac{z^m L_0}{\left[(x-X)^2 + (y-Y)^2 + z^2\right]^{(m+2)/2}}, \tag{4}$$

where z is the distance from the micro-LED to the target plane, (X, Y) are the coordinates of the LED in the (x, y) plane, and m is the number of particles. Based on the existing technical conditions in the laboratory, we set the half-light intensity angle $\theta_{1/2}$ of the micro-LED we are going to make to be about 70° and bring it into equation (2) to get its n value of 0.53. Based on the parameter value of n, our future setting of the distance from the light source to the biological tissue will allow us to calculate the light intensity of our single micro-LED. It can also be seen from equation (3) that the propagation distance has a large influence on the spatial light intensity distribution of the micro-LED, and the farther the propagation distance, the less light intensity is received and the smaller the effective surface spot area of the illuminated surface. In order to ensure the stimulation effect of the micro-LED on the nerve cells, the spacing between the light source and the nerve cells needs to be controlled. For this system, we have designed a micro-LED array irradiation method, so that the effect of superposition between light sources is also taken into account. As micro-LEDs are noncoherent light sources, the illumination of a region by two micro-LEDs is the superposition of the illumination of a single micro-LED. The superimposed illuminance can be obtained from

$$E_2(x,y,z) = \frac{2z^m L_0}{\left[(x-(d/2))^2 + y^2 + z^2\right]^{(m+2)/2}}, \tag{5}$$

where d is the distance between the centres of the two LEDs and the size of d should be reasonably controlled to ensure uniformity of illumination. When the LEDs are arranged in an array, the illuminance transmitted to a point $P(x, y, z)$ in the plane is the superposition of the illuminance of each light source in the array, and when arranged in a rectangular array of $N \times M$, equation (5) further yields the illuminance distribution of the array. When N and M are odd numbers,

$$E(x,y,z) = \sum_{n=-(N-1)/2}^{(N-1)/2} \sum_{l=-(M-1)/2}^{(M-1)/2} \cdot \frac{z^m L_0}{\left\{\left[x-(2n-1)(d_x/2)\right]^2 + \left[y-(2l-1)(d_y/2)\right]^2 + z^2\right\}^{(m+2)/2}}. \tag{6}$$

When N and M are even numbers,

$$E(x,y,z) = \sum_{n=-(N-2)/2}^{N/2} \sum_{l=-(M-2)/2}^{M/2} \cdot \frac{z^m L_0}{\left\{\left[x-(2n-1)(d_x/2)\right]^2 + \left[y-(2l-1)(d_y/2)\right]^2 + z^2\right\}^{(m+2)/2}}, \tag{7}$$

where d_x is the spacing of neighbouring LEDs in the x direction and d_y is the spacing of neighbouring LEDs in the y direction. In addition, for the whole system, the micro-LED arrays are eventually implanted into biological tissues, and the micro-LED arrays are ultimately implanted in biological tissues, and when the light source is illuminated, the illumination of the light source by the biological tissue fluid produces a dispersion phenomenon, which will be analysed in the next section.

From the theoretical derivation, it can be seen that for the design of the light source array, the distance between the centres of the two LED light sources and the light source (d) is a key factor that may affect the stimulation of the light source as well as the emission of the light source, which is proved in equations (6) and (7); at the same time, the distance from the light source to the biological tissues (z) and the intensity of the light (E) are also two important factors in equations (6) and (7).

2.2.2. Micro-LED Light Source Simulates Biological Irradiation Distribution. When a light source stimulates biological tissue, due to the special characteristics of biological tissue, photons propagate through the biological tissue in the process of interacting with the biological tissue microscopic particles. The scattering phenomenon occurs as a result of the interaction of photons with microscopic particles of biological tissue. The paths of photons in biological tissues are random and complex. Therefore, a Monte Carlo analysis is used to analyse the distribution of light in biological tissue. Upon entering the interior of a biological tissue, photons produce a random step, and an initial directional cosine representing represents the direction of motion. If the light source is incident vertically, its directional cosine in the x, y, z direction should be (0, 0, 1). Each time a photon is scattered, the direction cosine changes once. If the photon is still inside the tissue, it will travel according to the current step and direction cosine. If it is out of boundaries, the photon will be reflected or transmitted according to random sampling. If it is transmitted, the photon will be terminated; the photon will be scattered and absorbed after moving the distance of the current step, and the weight of the photon will be changed. If the weight of the photon is greater than the set photon termination threshold, the photon starts a new round of walking, and conversely, if the weight of the photon is less than the termination threshold, the Russian roulette method is used to determine whether the photon still has a chance to start a new round of tracking.

The scattering and absorption of photons occurring in biological tissues as well as the step size and direction of motion of photons are generated by random numbers on the basis of their probability distributions [18]. If the

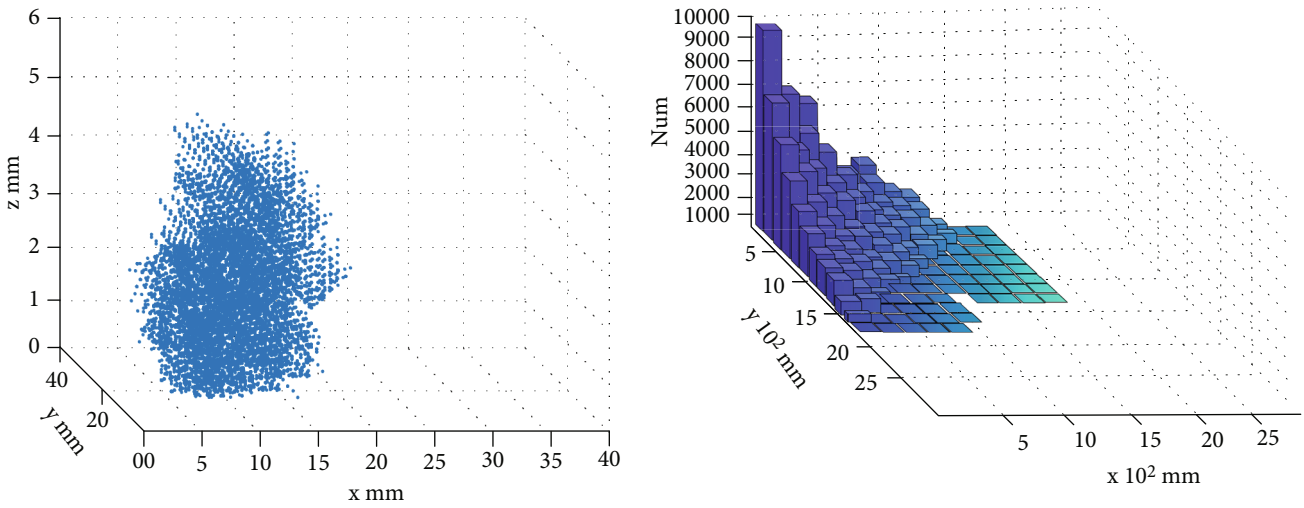

(a) (b)

FIGURE 4: Spatial distribution of energy absorbed by biological tissues: (a) distribution of energy received by biological tissues for $\beta = 0.5$; (b) distribution statistics for $\beta = 0.5$.

probability distribution of the variable x between $(x1, x2)$ is $P(x)$, the ε of the pseudorandom number between (0,1) is generated by computer; i.e., x is calculated by the following equation, and the random numbers are sampled during the simulation by the following equation.

$$\int_{x1}^{x2} P(x)dx = \varepsilon. \tag{8}$$

This is done in the following five steps:

(1) Photon random step sampling: the dimensionless distance a photon needs to travel to interact with the microscopic particles of biological tissue during its walk becomes the photon's step length. From the biological tissue action coefficient ρ_t,

$$\rho_t = \frac{-dP\left\{\varnothing \geq \varnothing'\right\}}{P\left\{\varnothing \geq \varnothing'\right\}d\varnothing'}. \tag{9}$$

The final collation gives a probability density function for the step size:

$$P(\varnothing) = \rho_t \exp\left(-\rho_t \varnothing\right). \tag{10}$$

Thus, there are sampling equations for random steps:

$$\varnothing = \frac{\mathrm{In}(\varepsilon)}{\rho_t}. \tag{11}$$

A random step can be thought of as a distance of $\varnothing$ through which photons pass before they interact with biological tissue in absorption and scattering.

(2) Sampling in the direction of photon scattering: scattering occurs when photons interact with biological tissue, and both the deflection angle $\theta(0 \leq \theta \leq \pi)$ and the azimuthal angle $\psi(0 \leq \psi \leq 2\pi)$ of scattering need to be randomly sampled, and the probability density function of the scattering angle is

$$P(\theta) = \frac{1-\beta^2}{4\pi\left(1+\beta^2-2\beta cos\theta\right)^{3/2}}, \tag{12}$$

where β is the anisotropy factor, where it is isotropic scattering at 0, forward scattering at values close to 1, and between 0.3 and 0.9 for biological tissues; the final random sampling equation for $\cos\theta$ is obtained as

$$\cos\theta = \frac{1}{2\beta}\left\{1+\beta^2-\left[\frac{1-\beta^2}{1-\beta+2\beta\epsilon}\right]^2\right\}, \beta \neq 0. \tag{13}$$

The directional angle sampling equation is $\psi = 2\pi\varepsilon$, and the newly obtained direction of motion of the photon is as follows:

$$\begin{aligned}
\rho_x{}' &= \frac{\sin\theta\left(\rho_x\rho_z\cos\psi - \rho_y\sin\psi\right)}{\sqrt{1-\rho_z{}^2}} + \rho_x\cos\theta, \\
\rho_y{}' &= \frac{\sin\theta\left(\rho_x\rho_z\cos\psi - \rho_y\sin\psi\right)}{\sqrt{1-\rho_z{}^2}} + \rho_z\cos\theta, \\
\rho_z{}' &= -\sin\theta\cos\psi\sqrt{1-\rho_z{}^2} + \rho_z\cos\theta.
\end{aligned} \tag{14}$$

If $|\rho_z| \geq 0.9999$, the new direction of the photon is then given by

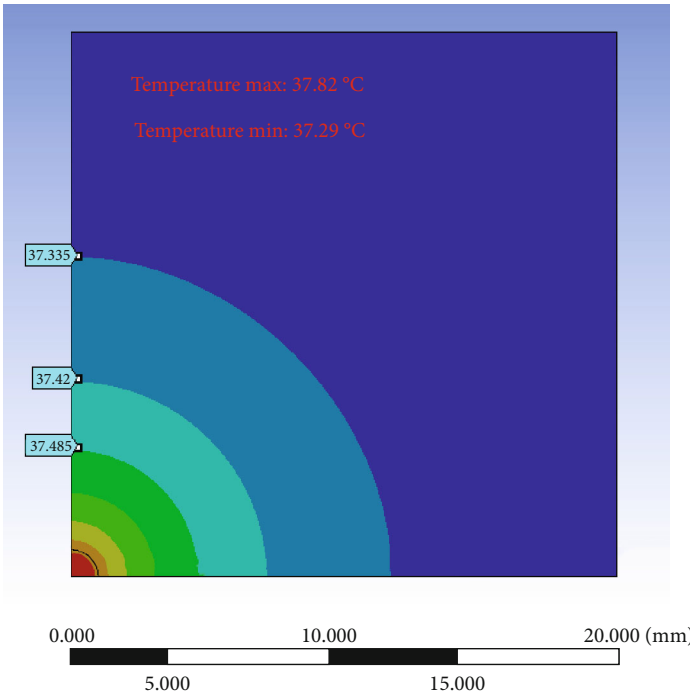

(a)

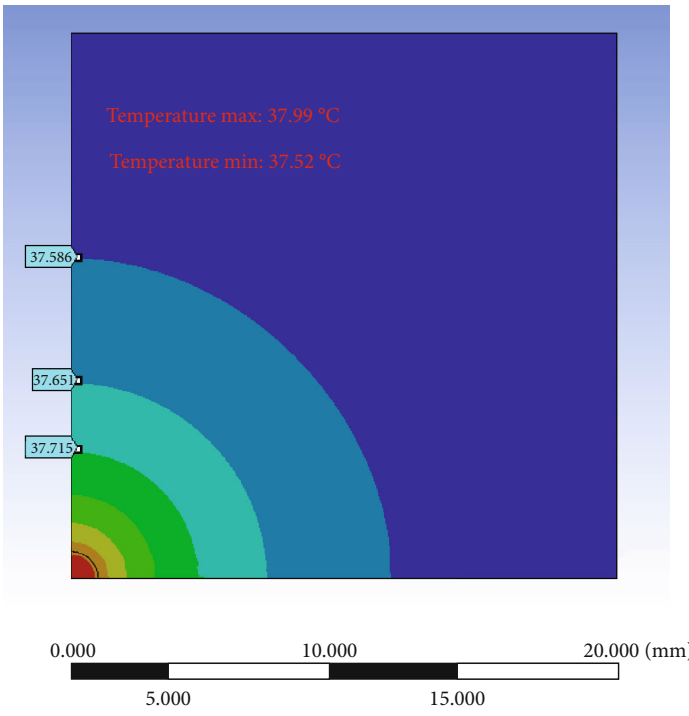

(b)

Figure 5: Continued.

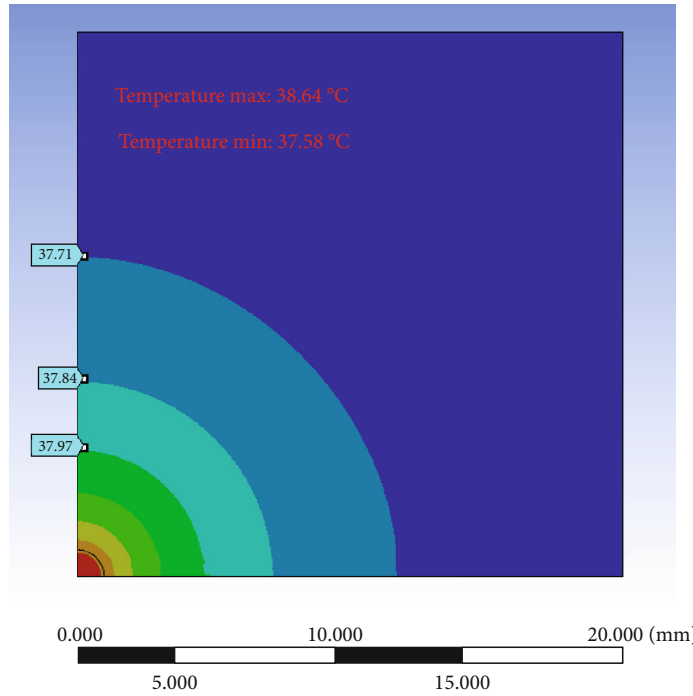

(c)

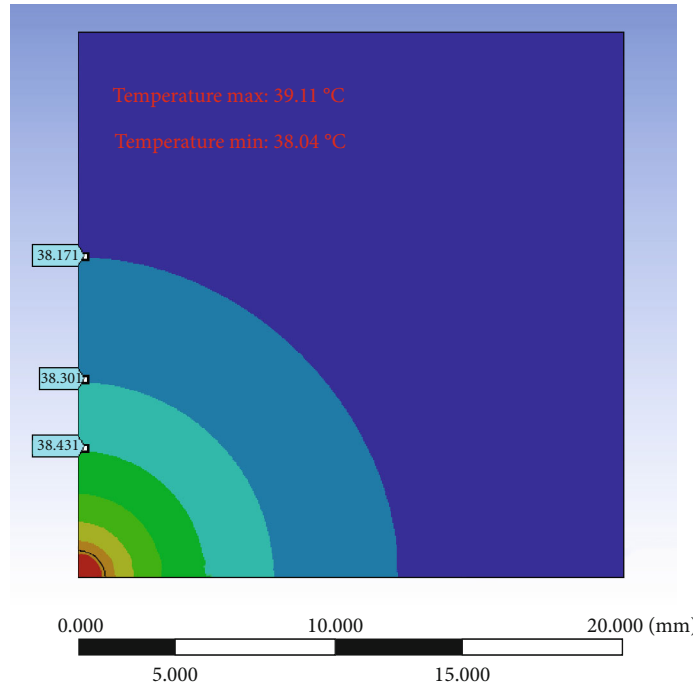

(d)

Figure 5: Results of the finite element method for the heat source term obtained by the Monte Carlo method: (a, b) solution process for 20 mW optical power, 30 s; (c) solution process for 40 mW optical power, 30 s; (d) solution process for 40 mW optical power, 50 s.

$$\begin{aligned} \rho_x' &= \sin\theta\cos\psi, \\ \rho_y' &= \sin\theta\sin\psi, \\ \rho_z' &= \mathrm{SIGN}(\rho_z)\cos\theta. \end{aligned} \tag{15}$$

(3) Photon emission: the light source emits photons, which have an initial position and an initial direction of motion, the direction of motion being represented by the direction cosine. The position information of the photon during transmission is represented by the coordinates of the Cartesian coordinate system, i.e., (x, y, z), and the direction cosine is labeled

as (ρ_x, ρ_y, ρ_z), encapsulating the position of the photon and its direction of motion as a photon packet, which is a Monte Carlo simulation. In order to simulate the energy decay of photons during transmission [19], an initial weight ω is set for each photon packet, which is set to 1 in this paper. For a collimated incident light source, the initial direction cosine of the photon is (0, 0, 1) and the initial position is (0, 0, 0); photons on the surface of biological tissue will first have a small portion of light specularly reflected; if the refractive index of biological tissue is $n1$, the refractive index of the medium adjacent to the tissue when the light source is incident is $n2$; accordingly, the specular reflectance is

$$R_{sp} = \frac{(n1 - n2)^2}{(n1 + n2)^2}. \tag{16}$$

After the photon incident, the photon weight is reduced by the specular reflection R_{sp}.

(4) Photon absorption: in order to facilitate the physical quantities to be simulated, the direction of incidence of the vertical light source is called the radial direction (r direction) and the direction of incidence of the light source is called the axial direction (z direction). A lattice system is established, dividing r and z into N lattices, respectively, and the weights of the photons absorbed during the simulation are passed through the lattice system and recorded in the absorption matrix. The absorption matrix gives the odds of a photon being absorbed at the position in the radial and axial directions. The photon energy flow rate can be obtained from the total number of photons and the lattice size

(5) Photon disappearance: when the photon weight is less than a threshold, Russian roulette is used to determine whether the photon can survive [22]. The computational coding was written in MATLAB to simulate the distribution of the light obtained in this environment. The transmission distribution of 10^4 photons in biological tissues was simulated with an absorption coefficient of 0.5 cm^{-1}, a scattering coefficient of 80 cm^{-1}, and a refractive index of 1.37 [22]. The photon absorption was calculated for an anisotropy factor (β) 0.5, and the incident light source was an infinitely fine beam. The simulation results are shown in Figure 4, from which it can be seen that the energy of the incident light is almost concentrated in a small area near the incident point and the photon absorption. When $\beta = 0.5$, the rate of decrease of the photon absorption in the R-axis is significantly faster than that in the z-axis. When $\beta = 0.5$, the rate of decrease of photon absorption in the R-axis is significantly faster than that in the z-axis, which is in general agreement with the conventional light diffusion results, while the simulation results are also consistent when β is equal to other values

Table 2: Thermal simulation results.

Light power	Time	Max. temperature	Min. temperature	Temperature difference
20 mW	30 s	37.833°C	37.289°C	0.533°C
20 mW	50 s	38.053°C	37.519°C	0.534°C
40 mW	30 s	38.644°C	37.577°C	1.067°C
40 mW	50 s	39.105°C	38.038°C	1.067°C

2.2.3. Analysis of Heat Generation from Micro-LEDs and Biological Tissue. The photothermal reaction between light source and biological tissue depends on the one hand on the irradiation parameters of the light source (e.g., distance between light source and biological tissue, distance between single light sources, light source radiation flux, combination of light source irradiation methods, wavelength, current, voltage, electrical power, and frequency) and on the other hand on the characteristic parameters of the biological tissue itself, including optical and thermal parameters. The optical parameters determine the distribution of light and the amount of light energy deposited in the tissue, while the thermal parameters determine the storage and transfer of heat within the biological tissue and the resulting temperature changes within the tissue. The parameters that determine the distribution of heat within biological tissues are the specific heat C (J/(g·°C)), density ρ (g/cm^3), and thermal conductivity K (W/cm·°C). At the same time, the thermal parameters of biological tissues are related to the size of the water content of the tissue as well as to the temperature. Ortner et al. proposed the following relationships between the thermal parameters of biological tissues and the water content of the tissue through experimental studies [23].

$$\begin{aligned} \rho &= S + W \left(\mathrm{g/cm^3}\right), \\ C &= 4.19 \times \left(0.37 + 0.67\frac{W}{\rho}\right) \quad (\mathrm{J/(g \cdot {}^\circ C)}, \\ K &= 4.19 \times \left(0.133 + 1.36\frac{W}{\rho}\right) (\mathrm{mW/cm \cdot {}^\circ C}). \end{aligned} \tag{17}$$

where S (g/cm^3) is the density of material other than water inside the tissue and W (g/cm^3) is the density of the water within the tissue. In addition to this, Jacques and Prahl have suggested that the biological tissue density is related to water content and have given a relationship between the two [24]. Gourlay et al. have also given a relationship between the thermal parameters of biological tissues and the internal tissue. Gourlay et al. also give a relationship between the thermal parameters of biological tissues and the internal water content and fat and protein content of the tissue [25]. In addition to the tissue water content, the temperature magnitude of the biological tissue also has an effect on the tissue thermal parameters. If the effect of temperature on the thermal properties of the tissue is not taken into account in the

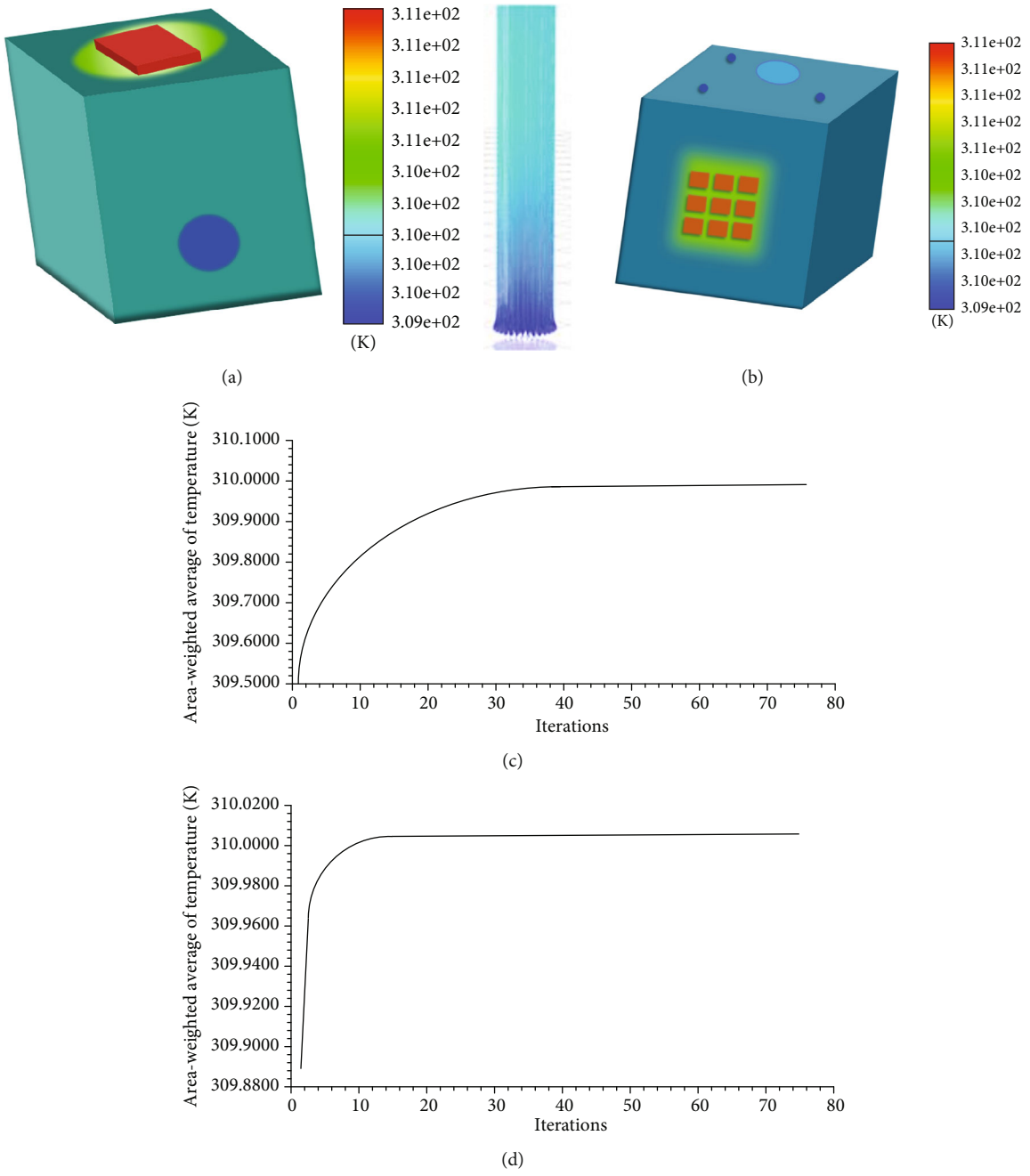

Figure 6: Combined light source and biological tissue simulation: (a, b) simulation results with a single light source; (c) steady-state results with a single light source; (d) steady-state results with an array of light sources.

calculations, some temperature compensation should be applied to the calculation process.

In addition to the thermal parameters of the biological tissue itself, the heat transfer process of the biological tissue has to be taken into account. There are three forms of heat transfer, which mainly include heat conduction, heat radiation, and heat convection. The total amount of heat generated by biological tissue when irradiated by a micro-LED and the final size of the tissue heat deposition are inextricably linked to the heat transfer process. The study of the photothermal effects on biological tissues requires a clear understanding of the energy generated by the light source

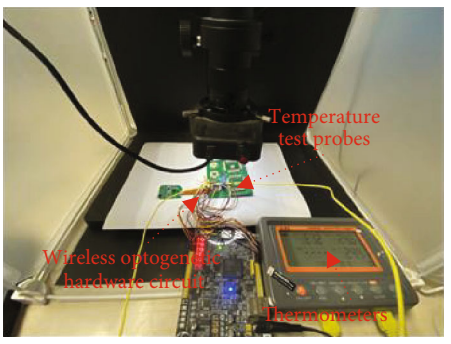

Figure 7: Temperature test platform.

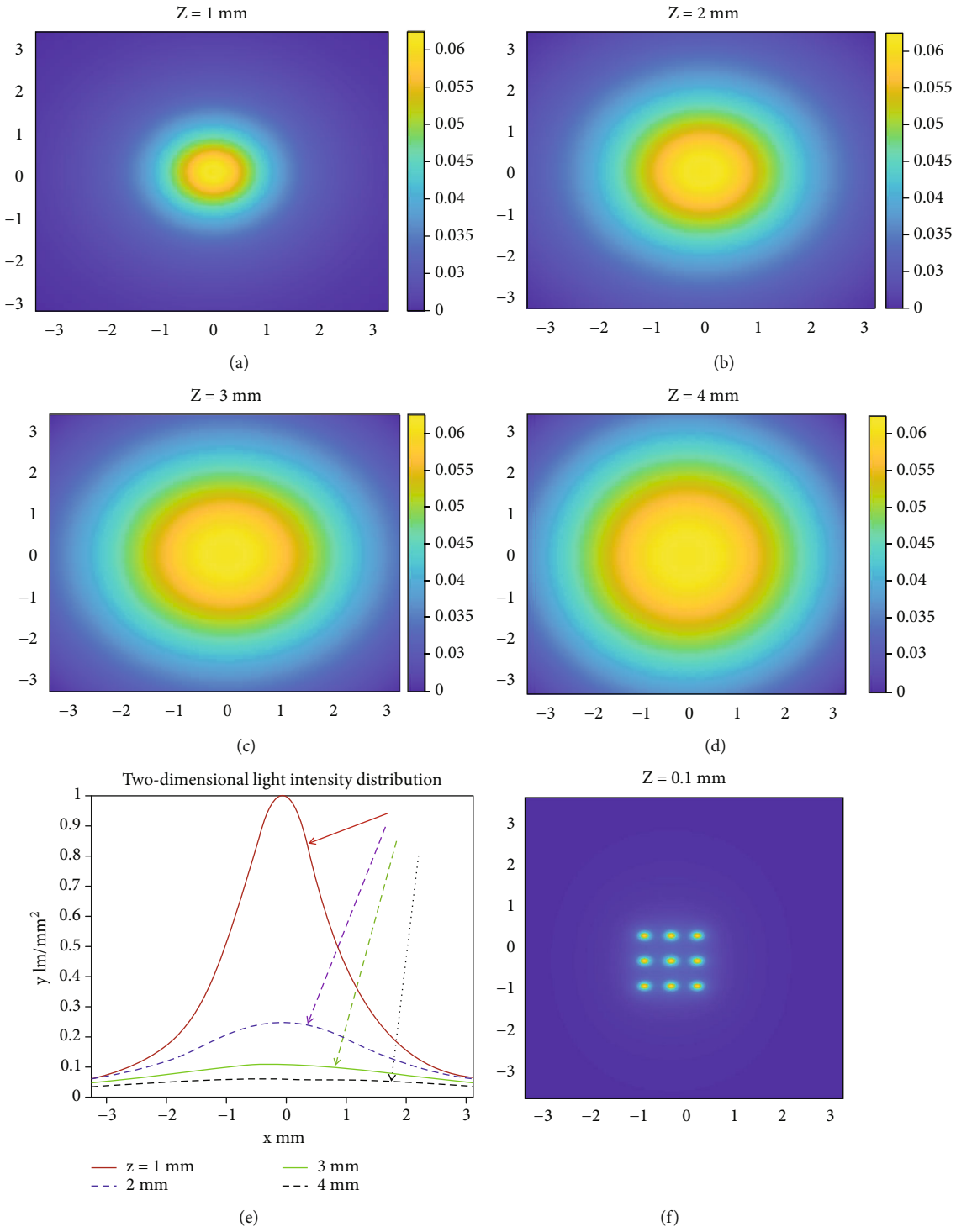

Figure 8: Continued.

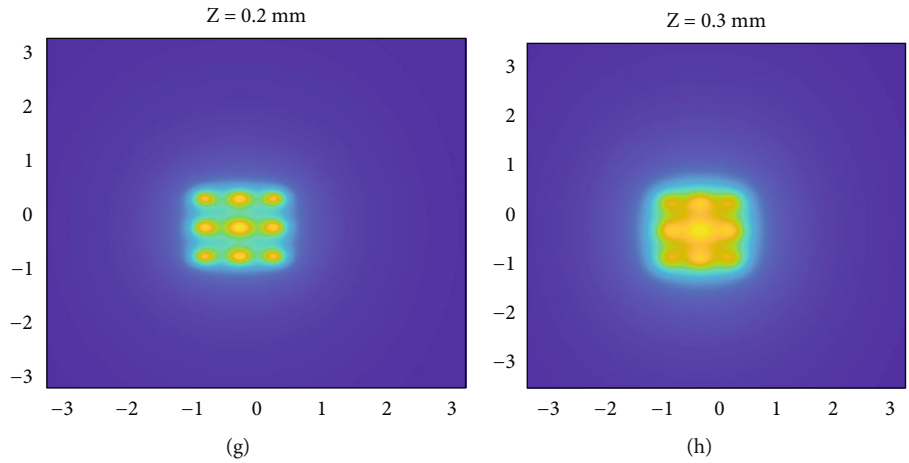

Figure 8: The simulated irradiation of single micro-LED and micro-LED array in biological tissues: (a–d) the dispersion distribution of the light source of a single micro-LED when it is 1 mm-4 mm away from the target neuron; (e) the statistics of the dispersion of the light source of (a–d); (f–h) the dispersion distribution of the array of micro-LED when it is 0.1 mm-0.3 mm away from the target neuron. It can be seen that the farther the neuron, the more diffuse the light is and the weaker the light intensity is at the target neuron.

and the final form of energy conversion. For living tissues, according to the law of conservation of energy, there are three main forms in which the energy obtained by the tissue after irradiation by a light source is present, as shown in the following equation.

$$Q = Q_{\text{store}} + Q_{\text{loss}} + Q_{\text{met}}. \tag{18}$$

The energy absorbed by the biological tissue Q_{store}, the loss of energy due to heat transfer within the biological tissue Q_{loss}, and the loss of energy due to metabolism within the biological tissue Q_{met}, Q is the energy gained by the biological tissue due to light exposure. Q_{store} is the decisive factor causing the temperature rise in the tissue. Q_{loss} consists mainly of the three forms of heat transfer previously described, heat conduction, heat radiation, and heat convection. The effect of thermal radiation is only apparent when the temperature is extremely high, and as the temperature rise from the photothermal interaction between the light source and the biological tissue is moderate, the effect of thermal radiation is negligible. The heat convection within the tissue is caused by blood perfusion and heat transfer based on blood flow. Since only the photothermal effect of the biological tissue in the isolated state is considered in this paper, the amount of the heat convection can be neglected, and similarly, the metabolic heat Q_{met} can be neglected. In this paper, the micro-LED light source parameters and the dynamic thermal properties of biological tissues are investigated. The heat transfer in biological tissues is described by the simplified Pennes heat transfer equation, which is based on the following equation:

$$\rho C \frac{\theta T}{\theta t} = \nabla(K \nabla T) + \text{WC}(T - T_{\vartheta}) + Q_{\text{met}} + Q. \tag{19}$$

The left-hand side of the equation represents the energy stored per unit volume within the tissue. The first term on the right side represents the heat energy loss due to temperature increase per unit volume, the second term represents the contribution of blood perfusion rate to the heat energy, the third term is the internal metabolic heat of the tissue, and the last term is the external heat source. The simulations in this paper are based on isolated liver tissue, and Q_{met} is ignored in the simulations, and the effect of blood perfusion is not considered. In order to determine a heat transfer process, in addition to the Pennes heat transfer equation, the initial and boundary conditions of the biological tissue model must be known, i.e., the definite solution conditions required in the solution of the partial differential equation. The initial condition is the initial temperature of the biological tissue, and the boundary condition is the state of heat transfer between the biological tissue and the surrounding environment. The most common forms of boundary conditions can be divided into three categories: the first category of boundary conditions, or the Dirichlet boundary conditions; the second category of boundary conditions, called the Neumann boundary conditions; and the third category of hybrid boundary conditions. The analytical solution to the Pennes equation is difficult to obtain and is generally solved numerically. The results of the solution of the heat source term obtained using the finite element method for the Monte Carlo method are shown in Figure 5.

From the graph, we measure the effect of the light source-related parameters optimised for the biological tissue temperature by the maximum temperature variation in the previous phase. The results of the simulation are tabulated in Table 2, and it can be seen that the variation range of our optimised system does not exceed 1.5 degrees Celsius with power and time.

In addition to the optical power and time, we have based this on a joint simulation of the photopolar array's own parameters, the distance to the biological tissue, and the spacing of the light sources in standard words. As shown in Figure 6, from these parameters, we can derive a more precise range of parameters for our photostimulation system, which provides a theoretical basis for the practical tests we conduct later.

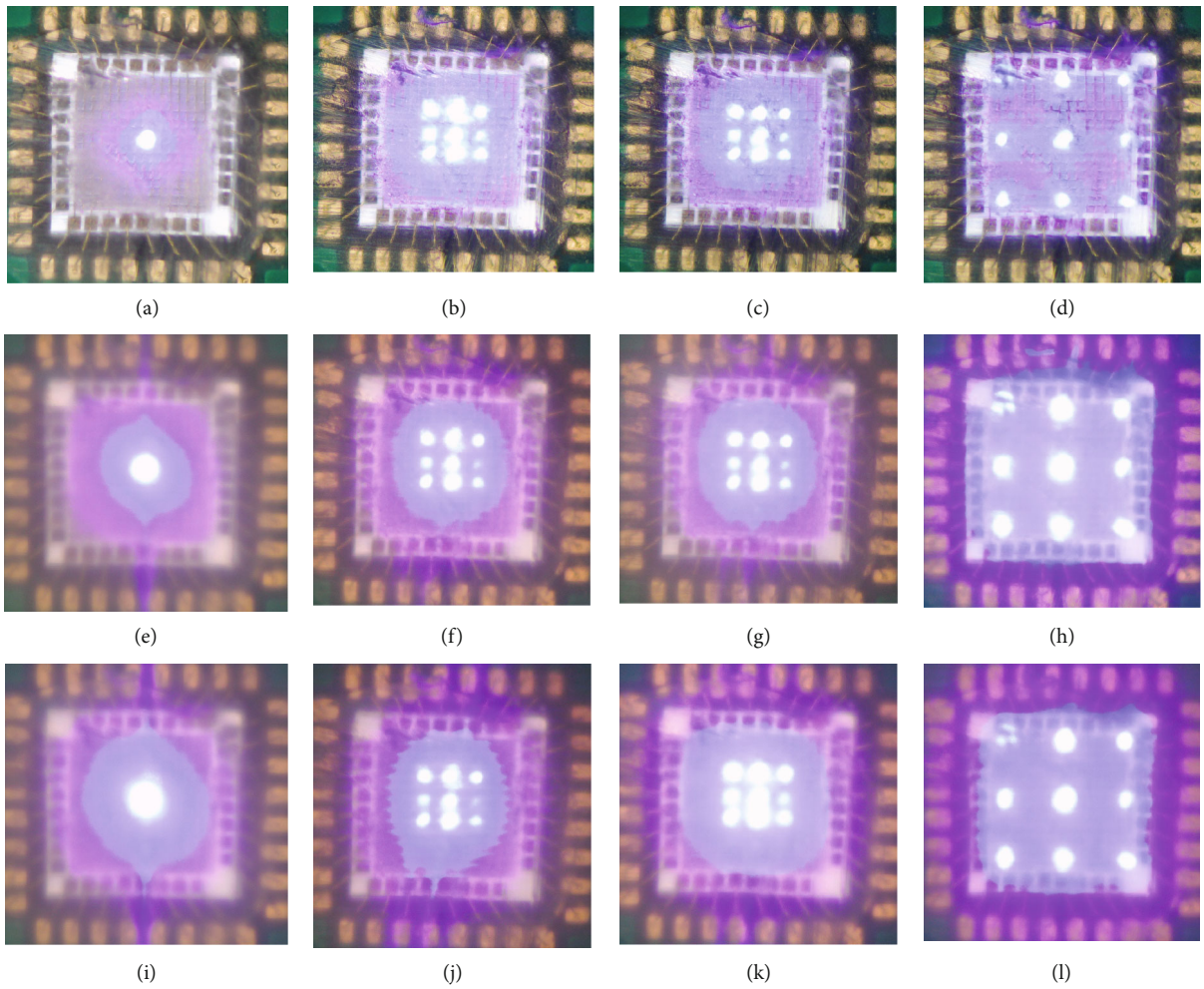

Figure 9: Micro-LED light source array test results: (a–d) the illumination of a single light source with 3×3 arrays at different spacing at 20 mA; (e–h) the illumination of a single light source with 3×3 arrays at 40 mA for a tissue distance of 1 cm; (i–l) the illumination of a single light source with 3×3 arrays at 40 mA for a tissue distance of 2 cm.

3. Construction of Experimental Platforms

The LEDs on the optical poles were originally designed to operate at 0-100 mA, but in practice, they are within 10 mA, which is about a tenth of the original design. The entire optogenetic circuit comes with a temperature measurement chip, TMP117, which is a high-precision, low-power digital temperature sensor that can measure temperature changes within 5 mm of the light source, while using a high-precision thermometer (model: AZ 88598 4ch K SD Logger) to measure the temperature of the light source surface contact and the surrounding temperature, the two thermometers achieve mutual correction. The two thermometers correct each other to give an accurate picture of the temperature change. The measurements are carried out in an enclosed space with a constant temperature of 28 degrees Celsius, using different parameters of the light source and continuous and pulsed irradiation. The entire temperature test platform is shown in Figure 7.

While for the overall experimental system as shown in Figure 7, primary isolated spiral ganglion cell cultures were obtained from newly born fetal rats as required by the design of this system and cultured in a similar way to that described in [26]. Briefly, pregnant female rats are cultured, and when the fetal rats are delivered, a portion of the spiral ganglion cells are surgically removed at the fetal rat ear location and placed in phosphate-buffered saline (PBS) for cryoprotection. Under aseptic conditions, 2-5 spiral ganglion cells from fetal mice were desliced, depending on the number of cells required. Using fine forceps and scissors, an incision is formed at the back of the ear, and once cut, the spiral ganglion cells will be separated, collected through a plastic pipette, and then gently transferred to a culture dish in digest containing trypsin for 20 minutes before being placed into PBS and washed several times. 0.5 ml of DNAase solution is added to the tissue solution. The DNAase solution can be used to remove possible DNA contaminants to avoid them interfering with the results of the experiment. Rub the cell surface through the pipette tip until there is no visible sign of tissue. These suspensions are slowly centrifuged for about 10 min, at which point, the resulting cell pellet becomes ready-made medium after removal in PBS. Coating

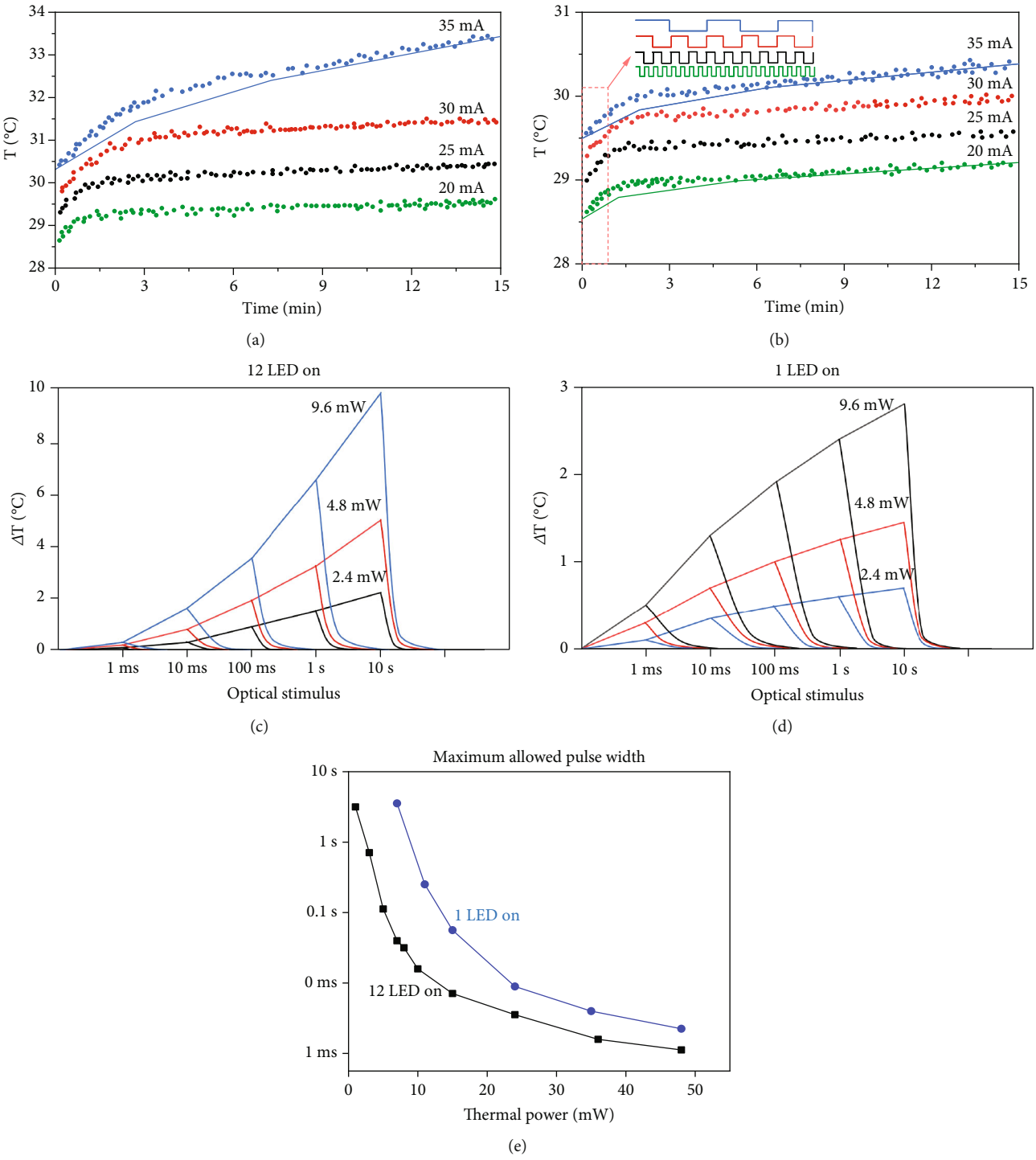

FIGURE 10: Test results of the photodiode array parameters. (a) Temperature variation curve for micro-LED array at different currents. (b) Temperature variation curve at different PWM. (c) Temperature variation at different power levels with 12 light sources lit. (d) Temperature variation at different power levels with a single light source lit. (e) Maximum permissible pulse width and duty cycle for a given power and temperature rise limit of 2 degrees Celsius.

the surface of the photopolar array with polylysine constructs a biosensor function that allows for highly sensitive and selective detection of target molecules. The whole process was completed with cell acquisition. The previously selected photosensitive protein+viral vector is then targeted and injected into the spiral ganglion cells, and the entire cell transfection is completed by 60 days of culture, culminating in precise stimulation using our self-developed optogenetic hardware results, while the system is mainly completed with temperature monitoring, achieving optimal temperature limits through temperature monitoring, light sources, and biological tissue.

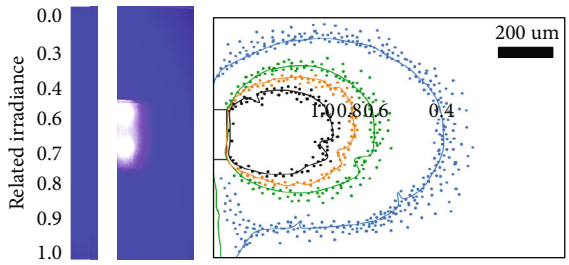

FIGURE 11: Micro-LED array temperature test results and quantitative comparison between experimental profiles (lines) and simulated profiles (dots).

4. Results and Discussion

4.1. Optical System Simulation Results. The designed micro-LED array was experimentally tested by comparing the light source simulation algorithm designed in Figure 8, setting the light source current at 20 mA in Figures 9(a)–9(d), lighting a single light source and a 3×3 light source array in the micro-LED light source, and setting the light source array with different pitches of 76 μm, 144 μm, and 212 μm light source arrays. When simulated close to the biological tissue at 1 cm and varying the current of the light source to 40 mA, the projection diagram of the array of light sources is shown in Figures 9(e)–9(h). When close to the biological tissue for 2 cm, the projection diagram is shown in Figures 9(i)–9(l). It can be seen experimentally that the distance between the pair and the light source and the distance between the light source and the tissue and at the specified light intensity are consistent with the simulation results. It should be noted that this experiment was conducted in customised culture dishes. Therefore, the safety of both the light source and the cells can be disregarded.

In the 3×3 array of light poles, different drive currents were designed to observe the temperature change under the drive circuit, and it can be found that the temperature change for 15 minutes at a drive current of 20 mA, 25 mA, 30 mA, and 35 mA can be seen that the overall temperature change is basically in a steady state within the change range of 1-2 degrees Celsius, as shown in Figure 10(a). The circuit from which we set the light sources is controlled differently at 35 mA by varying the duty cycle, and the temperature change can be seen as steady state in Figure 10(b). When lighting 12 light sources and a single light source, the change in temperature is within 2 degrees Celsius at different light powers as seen in Figures 10(c) and 10(d). This is consistent with the results of the previous simulation in Figures 5 and 6. When we specify a range of 2 degrees Celsius to look backwards at the limits of the light source at maximum PWM, as shown in Figure 10(e), we can see that the maximum allowable pulses of the light source include the range we set.

4.2. Photothermal System Simulation Results. The micro-LED array used in Figures 9–11 was temperature tested against simulated biological tissues. Firstly, diffusion experiments were carried out on the side of the light source to verify the diffusion effect of the light source against the biological tissues as shown in Figure 11. Thus, the photothermal model designed in this system achieves consistency between the algorithm modelling and the actual experiment. It should be noted that the results of pulse width modulation for different frequency designs are given in Figure 10(b), and the light stimulation in this paper is pulsed, which can be interpreted as a constant light mode when the pulse width modulation duty cycle reaches one hundred percent.

4.3. Discussion. Experiments were designed from three aspects, optical modelling, optical diffusion modelling, and photothermal modelling, to investigate the relationship between the final temperature (T) in terms of elements such as light source current (I), optical power (P), pulse width modulation (PWM), illumination mode (M), distance between light sources (R), distance from light source to biological tissue (D), and scattering properties of the light source (S). We have designed the function for this system as follows:

$$T = f(I, P, PWM, M, R, D, S). \tag{20}$$

We wish we had modelled optogenetic physics with more parameters. In addition to this, we have also conducted research from a cell culture perspective, using photolithography and using photovoltaic technology to study a customised culture dish-based cell culture system. Photolithography, spin-coating, and masking techniques will be used to achieve a more refined design of the culture dish arrays, and ultimately, the cells will be cultured in the designed culture dish arrays. Precise control of cells will be accomplished through this technology. And in the process of these designs, the cell temperature as well as the temperature variation of the whole hardware determines the feasibility of the whole experiment. This temperature issue is addressed by the individual models designed for this system.

5. Conclusion

We consider this work to be a more detailed study of the implementation of optoelectronics, integrated circuits, artificial intelligence, and physical modelling, and it leads to a number of targeted conclusions from the diagrams that precede this system. For the sake of simplicity, we will summarise four conclusions:

(1) We have designed a wireless optogenetics micro-LED array hardware circuit and a wireless power supply circuit, with the micro-LED array controlled at 60 m × 60 m

(2) We have designed optical array models for the hardware, scattering and absorption models for light sources and biological tissues, and a heat transfer model for light sources and biological tissues. The entire model aligns with the hardware test results. This comprehensive physical model has facilitated research in optogenetic photothermal modelling

(3) In the future, we hope to conduct algorithmic research in machine learning specifically for certain

parameters, enabling us to predict electrophysiological parameters

(4) The proposed method's application can be extended to implantable neural interfaces and any wireless neuromodulation strategies such as photothermal, photoacoustic, and magnetothermal, where a remote control over photothermal effect is required

We believe that the study of micro-LED photopolar arrays with photosensitive proteins and their reliability will continue to improve, but with the effective use of our light sources, the right stimulation protocols can all be used without significant heating of the tissue.

Data Availability

The data that support the findings of this study are available from the corresponding author upon reasonable request.

Conflicts of Interest

The authors declare no conflicts of interest.

Authors' Contributions

Yanping Ji and Chuanzhen Liu did the literature study and analysis. Yanping Ji and Jiawei Li wrote the manuscript. Mengyi Zheng and Wensi Wang designed the illustrations. All reviewed the illustrations, and all reviewed critically the manuscript.

Acknowledgments

This study was supported by the Beijing Science and Technology New Star Project, with project number 20230484450.

Supplementary Materials

Supplementary 1. Figure S1 shows the light source array end of the whole wireless optogenetic circuit, which mainly includes 8∗8 micro-LED array and temperature sensing chip TMP117. It is mainly on the flexible circuit board, which is the implantable part.

Supplementary 2. Figure S2 shows the entire wireless optogenetic circuit control circuit, mainly including wireless energy transmission circuit in the receiving circuit, control circuit nRF52832, and driver circuit LP5036. The main mode of operation is the receiving circuit to receive wireless energy, which will be converted into 3.3 V voltage on the control circuit and driver circuit power supply. The control circuit controls the driver circuit to complete the micro-LED array to achieve different illumination methods.

References

[1] S. Makowski, J. S. Knutson, J. Chae, and P. Crago, "Neuromuscular electrical stimulation to augment reach and hand opening after stroke," in *2011 Annual International Conference of the IEEE Engineering in Medicine and Biology Society*, pp. 3055–3058, Boston, MA, USA, 2011.

[2] E. W. Sellers, D. B. Ryan, and C. K. Hauser, "Noninvasive brain-computer interface enables communication after brainstem stroke," *Science Translational Medicine*, vol. 6, no. 257, article 257re7, 2014.

[3] "Web resource: Changchun New Industry Optoelectronics Technology Co., Ltd, a subsidiary of Changchun Institute of Optics, Chinese Academy of Sciences, Optogenetics and Neuro-Optics Lasers product page," http://www.cnilaser.com/.

[4] N. Grossman, K. Nikolic, C. Toumazou, and P. Degenaar, "Modeling study of the light stimulation of a neuron cell with channelrhodopsin-2 mutants," *IEEE Transactions on Biomedical Engineering*, vol. 58, no. 6, pp. 1742–1751, 2011.

[5] S. Kleinlogel, K. Feldbauer, R. E. Dempski et al., "Ultra light-sensitive and fast neuronal activation with the Ca2+-permeable channelrhodopsin CatCh," *Nature Neuroscience*, vol. 14, no. 4, pp. 513–518, 2011.

[6] K. Nikolic, N. Grossman, M. S. Grubb, J. Burrone, C. Toumazou, and P. Degenaar, "Photocycles of channelrhodopsin-2," *Photochemistry and Photobiology*, vol. 85, no. 1, pp. 400–411, 2009.

[7] J. Chao, S. Ram, E. S. Ward, and R. J. Ober, "Ultrahigh accuracy imaging modality for super-localization microscopy," *Nature Methods*, vol. 10, no. 4, pp. 335–338, 2013.

[8] L. Lu, P. Gutruf, L. Xia et al., "Wireless optoelectronic photometers for monitoring neuronal dynamics in the deep brain," *Proceedings of the National Academy of Sciences of the United States of America*, vol. 115, no. 7, pp. E1374–E1383, 2018.

[9] J. Mattis, K. M. Tye, E. A. Ferenczi et al., "Principles for applying optogenetic tools derived from direct comparative analysis of microbial opsins," *Nature Methods*, vol. 9, no. 2, pp. 159–172, 2012.

[10] J. Vierock, S. Rodriguez-Rozada, A. Dieter et al., "BiPOLES is an optogenetic tool developed for bidirectional dual-color control of neurons," *Nature Communications*, vol. 12, no. 1, p. 4527, 2021.

[11] F. Zhang, L. P. Wang, M. Brauner et al., "Multimodal fast optical interrogation of neural circuitry," *Nature*, vol. 446, no. 7136, pp. 633–639, 2007.

[12] W. Hong, J. Lee, D. Kim et al., "Computational thermal analysis of the photothermal effect of thermoplasmonic optical fiber for localized neural stimulation in vivo," *Electronics*, vol. 10, no. 2, p. 118, 2021.

[13] N. S. S. Mousavi, K. B. Ramadi, Y.-A. Song, and S. Kumar, "Plasmonics for neuroengineering," *Communications Materials*, vol. 4, no. 1, 2023.

[14] R. Chen, G. Romero, M. G. Christiansen, A. Mohr, and P. Anikeeva, "Wireless magnetothermal deep brain stimulation," *Science*, vol. 347, no. 6229, pp. 1477–1480, 2015.

[15] N. Mcalinden, D. Massoubre, E. Richardson et al., "Thermal and optical characterization of micro-LED probes for in vivo optogenetic neural stimulation," *Optics Letters*, vol. 38, no. 6, pp. 992–994, 2013.

[16] P. Tan, L. He, Y. Huang, and Y. Zhou, "Optophysiology: illuminating cell physiology with optogenetics," *Physiological Reviews*, vol. 102, no. 3, pp. 1263–1325, 2022.

[17] A. Albouy and L. Zhao, "Lambert's theorem and projective dynamics," *Philosophical Transactions of the Royal Society A:*

Mathematical, Physical and Engineering Sciences, vol. 377, no. 2158, 2019.

[18] Y. Tokuyoshi and T. Harada, "Hierarchical russian roulette for vertex connections," *ACM Transactions on Graphics*, vol. 38, no. 4, pp. 1–12, 2019.

[19] A. Soltan, B. Mcgovern, E. Drakakis et al., "High density, high radiance μ LED matrix for optogenetic retinal prostheses and planar neural stimulation," *IEEE Transactions on Biomedical Circuits and Systems*, vol. 11, no. 2, pp. 347–359, 2017.

[20] M. Kadobianskyi, I. N. Papadopoulos, T. Chaigne, R. Horstmeyer, and B. Judkewitz, "Scattering correlations of time-gated light," *Optica*, vol. 5, no. 4, 2018.

[21] J. Marini, L. D. Bell, and F. Shahedipour-Sandvik, "Monte Carlo simulation of III-nitride photocathodes," *Journal of Applied Physics*, vol. 123, no. 12, 2018.

[22] Y. Narukawa, M. Ichikawa, D. Sanga, M. Sano, and T. Mukai, "White light emitting diodes with super-high luminous efficacy," *Journal of Physics D: Applied Physics*, vol. 43, no. 35, article 354002, 2010.

[23] V. K. Ortner, A. Sahu, M. Haedersdal, M. Rajadhyaksha, and A. M. Rossi, "Assessment of laserinduced thermal damage in fresh skin with ex vivo confocal microscopy," *Journal of the American Academy of Dermatology*, vol. 84, no. 1, pp. e19–e21, 2021.

[24] S. L. Jacques and S. A. Prahl, "Modeling optical and thermal distributions in tissue during laser irradiation," *Lasers in Surgery and Medicine*, vol. 6, no. 6, pp. 494–503, 1987.

[25] E. Gourlay, P. GLé, S. Marceau, C. Foy, and S. Moscardelli, "Effect of water content on the acoustical and thermal properties of hemp concretes," *Construction and Building Materials*, vol. 139, pp. 513–523, 2017.

[26] K. N. Darrow, M. C. Slama, E. D. Kozin et al., "Optogenetic stimulation of the cochlear nucleus using channelrhodopsin-2 evokes activity in the central auditory pathways," *Brain Research*, vol. 1599, pp. 44–56, 2015.